Modeling interactions between tides, storm surges, and river discharges in the Kapuas River delta

Joko Sampurno[1,2], Valentin Vallaeys[1], Randy Ardianto[3], Emmanuel Hanert[1,4]

[1]Earth and Life Institute (ELI), Université Catholique de Louvain (UCLouvain), Louvain-la-Neuve, 1348, Belgium
[2]Department of Physics, Fakultas MIPA, Universitas Tanjungpura, Pontianak, 78124, Indonesia
[3]Pontianak Maritime Meteorological Station, Pontianak, 78111, Indonesia
[4]Institute of Mechanics, Materials and Civil Engineering (IMMC), Université Catholique de Louvain (UCLouvain), Louvain-la-Neuve, 1348, Belgium

Correspondence to: Joko Sampurno (joko.sampurno@uclouvain.be, jokosampurno@physics.untan.ac.id)

Abstract. The Kapuas River delta is a unique estuary system on the west coast of the island of Borneo, Indonesia. Its hydrodynamics is driven by an interplay between storm surges, tides, and rivers discharge. These interactions are likely to be exacerbated by global warming, leading to more frequent compound flooding in the area. The mechanisms driving compound flooding events in the Kapuas River Delta remain, however, poorly known. Here we attempt to fill this gap by assessing the interactions between river discharges, tides, and storm surges and how they can drive a compound inundation over the riverbanks, particularly within Pontianak, the main city along the Kapuas River. We simulated these interactions using the multi-scale hydrodynamic model SLIM. Our model correctly reproduces the Kapuas River's hydrodynamics and its interactions with tides and storm surge from the Karimata Strait. We considered several extreme scenario test cases to evaluate the impact of tide-storm-discharge interactions on the maximum water level profile from the river mouth to the upstream part of the river. Based on the maximum water level profiles, we could divide the second largest distributary of the Kapuas River's stream into three zones, i.e., the tidally-dominated region (from the river mouth to about 4 km upstream), the mixed-energy region (from about 4 km to about 46 km upstream) and the river-dominated region (beyond 46 km upstream). Thus, the local water management can define proper mitigation for handling compound flooding hazards along the riverbanks by using this zoning category. The model also successfully reproduced a compound flooding event in Pontianak, which occurred on 29 December 2018. For this event, the wind-generated surge appeared to be the dominant trigger.

1. Introduction

Global warming leads to more frequent tropical storms, rising sea levels, and more intense rainfalls, which all concur in increasing the occurrence of compound flooding events in a coastal area and its surrounding environment (Bevacqua et al.,

2020). Such disasters are impacting the lives of more and more people worldwide (Moftakhari et al., 2015). Compound flooding occurs when dry low-lying land (over a coastal area) is flooded by water from the ocean and the river. Compound

30 flooding is driven by the interaction between a coastal inundation and a riverine inundation. The former happens from the seaward direction due to high (spring) tides and storm surges, while the latter occurs from the landward due to high discharges from upstream rivers. Coastal communities, which have been growing in population over the past decades, have become increasingly vulnerable to those events. Cities located along an estuary are at the crossroad between the ocean and the river catchment, hence particularly vulnerable (Herdman et al., 2018; Vitousek et al., 2017; Zhang and Liu, 2017).

35 One of the most significant drivers that can trigger compound flooding over a coastal area are storm surges (Herdman et al., 2018; Zijl et al., 2013). A storm surges are defined as the difference between the observed water level and the expected water level that results from tidal dynamics in a coastal area. A storm surge effect on usual tidal dynamics is the altered timing of high and low water through non-linear processes (Zijl et al., 2013). A storm surge is composed of low- and high-frequency components (Spicer et al., 2019). The former modifies the non-tidal water level, and the latter represents a tide-surge interaction

40 during the event. A storm surge is generally quantified by the skew surge (Giloy et al., 2019), which is a tidal cycle average measurement—the difference between the observed height and the expected height. It reflects the level of surge generated over a tidal cycle. To mitigate compound flooding hazards in a coastal area, storm surge is a critical component that should always be taken into account.

Several factors must be considered regarding the assessment of compound flooding risks in a river delta. The first factor is the

45 coincidence of the sources (Herdman et al., 2018), which means there is a possibility for the delta to receive an extreme flow from the upstream, while, at the same time, there could be an intense surge occurring in the tide or excessive rainfall over the coastal area. The second factor is the dependency and interdependency of the sources, indicating whether the interaction between these sources (extreme flows, tides, and excessive rainfall) could significantly impact the inundation processes (Bilskie and Hagen, 2018; Herdman et al., 2018; Santiago-Collazo et al., 2019). Other important factors include the vegetation

50 properties along the riverbanks that resist the flow of water; the vegetative properties over the estuary that reduce the momentum transfer of wind; the landscape characteristics of the coastal area; and how they interacted with each other (Twilley et al., 2016).

Flooding events in a delta area can be simulated and assessed using hydrodynamic models (Deb and Ferreira, 2017; Olbert et al., 2017; Patel et al., 2017). The most useful models are those that can seamlessly simulate the processes occurring along the

55 land-sea continuum, which corresponds to the area encompassing the coast, the estuary, and the river channels. Such models allow for a study of past flooding events and an assessment of flood mitigation strategies (Vu and Ranzi, 2017). However, realistic input variables and forcing are needed to create an accurate physics-based hydrodynamic model. Since the processes

that drive compound flooding are three-dimensional, a 3D model is the most appropriate tool to evaluate the event. However, the use of a 3D model generally requires high computational costs. As an alternative, two-dimensional models are a good compromise between physical realism and computational costs, particularly for shallow and well-mixed domains (Huybrechts et al., 2010; Néelz, 2009). By reducing the physical complexity of the model, it is possible to increase the horizontal resolution; and hence, the model can better represent the system topography.

As an archipelago country with about 100,000 km of coastlines, Indonesia is faced with significant coastal flooding risks (World Meteorological Organization, 2021). Indonesian coastal flood hazards are classified as high (Think Hazard - Indonesia, 2022). It means that the potentially damaging waves are expected to flood the coasts at least once every ten years. Based on this risk and concerns about the impact of climate change in the future, a hazard assessment study in Indonesian low-lying coastal areas (such as deltas) is become critical for Indonesian water management authorities. One area in Indonesia that is vulnerable to coastal or even compound flooding is the Kapuas River delta. In this delta, flooding events happen more than once a year (Wells et al., 2016). Unfortunately, there is no previous study addressing the process that underlies the flood events in there. The previous study (Hidayat et al., 2014) successfully evaluated the inundation frequency, but only for the upstream area and did not evaluate the underlying process. Therefore, this study attempts to fill in the gap and provide the first compound flood assessment in the area.

This paper investigates the interaction between tides, storm surges, and river discharges in the Kapuas river estuary and its surrounding area. We use a 2D hydrodynamic model to simulate the interaction between these driving forces and their effects on the compound flooding in the Kapuas River delta, particularly in Pontianak. Then, we create a detailed flood assessment, determine the area's extent, and calculate the inundation depth. As a case study, we implemented the model explicitly to a compound flooding event on 29 December 2018.

2. Material and Method

2.1 Area of interest

The Kapuas River flows from the center of the Borneo island (Indonesia) toward the Karimata Strait on the west coast (Fig. 1). The river is one of the longest island's rivers in the world, with a length of about 1,143 kilometers (Goltenboth et al., 2006). The Kapuas river basin is located on the equator with high air temperature and humidity throughout the year. The river basin spreads over about 8.28×10^4 km^2, with about 66.7% of it consisting of forests (Wahyu et al., 2010). The topography of the river comprises hills over its upstream and plain over its downstream. The river flows into the Karimata Strait through five major branches (MacKinnon et al., 1996).

The Kapuas Kecil is the second largest distributary of the Kapuas. The river branch starts from a Kapuas branch at the Rasau Jaya district and ends at the estuary area in the Jungkat district. In the middle of its streamflow (about 20 km before the river mouth), the Landak tributary joins the Kapuas Kecil. The junction is located in the city of Pontianak, the capital of the province of West Kalimantan, Indonesia, placing the urban area at the highest risk of flooding among other areas along the Kapuas riverbanks.

Pontianak is the most populated urban area on the west coast of Borneo island, with a population of about 600,000 people that keeps increasing. The city is located on low-lying land and has 61 canals spread across the area. Most of these canals flow in the Kapuas Kecil River (Kondisi Geografis Kota Pontianak, 2021). As a consequence of its geographical situation, the city often experiences inundations.

2.2 Hydrodynamic model

The interplay between the river discharges, the tides, and wind surges from the sea and their effect on the inundation processes in Pontianak is investigated by using the Second-generation Louvain-la-Neuve, Ice-ocean Model (SLIM, https://www.slim-ocean.be/). The model equations are discretized with the discontinuous Galerkin finite element method. The model uses an unstructured mesh, whose resolution can vary in space. The model has successfully been applied to several areas, such as the Great Barrier Reef (Lambrechts et al., 2010), the Mahakam Delta (Pham Van et al., 2016), the Scheldt Estuary (Gourgue et al., 2013), and the Columbia River (Vallaeys et al., 2018).

Here, we use the wetting-drying barotropic version of SLIM that solves the conservative form of the Shallow Water Equations (SWE):

$$\frac{\partial H}{\partial t} + \nabla \cdot \boldsymbol{U} = 0 \tag{1}$$

$$\frac{\partial \boldsymbol{U}}{\partial t} + \nabla \cdot \left(\frac{\boldsymbol{U}\boldsymbol{U}}{H}\right) + f\boldsymbol{e_z} \times \boldsymbol{U} - \nabla \cdot (\upsilon\nabla\boldsymbol{U}) = \alpha gH\nabla(H-h) - \frac{Cd}{H^2}|U|U + \frac{1}{\rho}\tau_{wind} - \frac{H}{\rho}\nabla p_{atm} \tag{2}$$

where $\boldsymbol{U} = H\boldsymbol{\bar{u}}$ is the horizontal transport, H is the water column height, h is the bathymetry, t is the time, and $\boldsymbol{\bar{u}} = (u,v)$ is the depth-averaged horizontal velocity. α is a constant that is set to zero over dry elements and one over wet elements (Le et al., 2020), ∇ is the horizontal gradient operator, $g = 9.81$ m/s^2 is the gravitational acceleration, Cd is the bulk drag coefficient, f is the Coriolis parameter, $\boldsymbol{e_z}$ is the vertical unit vector pointing upward, υ is the horizontal eddy viscosity, τ_{wind} is the wind stress, and ∇p_{atm} is the atmospheric pressure gradient.

The model equations are solved using a wetting-drying algorithm with an implicit time-stepping scheme. With this algorithm, a mesh element can be defined as wet or dry. It requires a procedure that guarantees that the water column height (H) is always positive at the end of the time step to solve the equations. To achieve that, we set first a threshold $h*$ that indicates the water height below which an element is assumed to be dry (here $h* = 0.1$ m). Then, we define a parameter representing the total water column height on an element as a combination of maximum water level and minimum bathymetry: $s = \max(\eta) + \min(h)$. When s is smaller than $h*$, gravity will be canceled on the element so that the artificial gradient of surface elevation would not remove water from an already-dry element ($\alpha = 0$). On the contrary, if s is greater than $h*$, then the gravitational force will be preserved as usual ($\alpha = 1$). The transition between $\alpha = 0$ and $\alpha = 1$ occurs smoothly. More details about this procedure can be found in Le et al. (2020).

2.3 Model setup

Before creating the model, we first define a domain covering both the ocean and the Kapuas River Delta. Since we focused on evaluating the impact of tide-surge-discharge interaction on extreme water levels along the Kapuas Kecil branch (particularly in Pontianak), we leave out several distributaries that may not significantly influence that dynamics, such as the Southern Kubu branch. Next, we mesh the domain, set the bathymetry and the bulk drag coefficient, define the boundary conditions (surface elevation and velocity), and finally impose some forcings. After the model is created and run successfully, we validate the results using observational data.

Here, we generate a multi-scale mesh of the entire domain by using the mesh-generation algorithm of Remacle and Lambrechts (2018). The mesh consists of 206,359 triangular elements. Fine mesh elements are used to accurately represent inundation events over the land area of Pontianak and along the Kapuas riverbanks, while the coarser mesh elements are used far away from the delta. The mesh resolution reaches 50 m along the Kapuas riverbanks and over the city of Pontianak. It decreases to 10 km in the middle of the Karimata Strait (Fig. 1).

The bathymetry is created from a combination of three different data sources. The first is the river and estuary bathymetry obtained from the Indonesian Navy (Kästner et al., 2019) with a 100×100 m grid resolution. The second is the Karimata Strait bathymetry, obtained from BATNAS (BATimetri NASional, 2021) with a 180×180 m grid resolution. The last is the digital elevation model from DEMNAS (DEMNAS, 2022) with 0.27-arcsecond resolution. The Karimata Strait bathymetry shows that the strait is shallow (less than 100 m) and relatively flat (Fig. 2). On the other hand, the bathymetry of the river is more heterogeneous. The river is shallow in the estuary but deeper in the middle stream. The depth ranges from 1 m (in the estuary area) to 40 m in the middle stream area (Kästner et al., 2017). The Kapuas Kecil River, which flows through Pontianak, has a depth that decreases from 15 m in the middle stream to 1 m in the river mouth.

The wind velocity and the atmospheric pressure data are the ERA5 reanalyzes dataset obtained from the European Canter for Medium-Range Weather Forecast (ECMWF). The data have a spatial resolution of 31 km (Hersbach et al., 2020), while the temporal resolution is hourly and available at 137 vertical levels (0 to 80 km from the surface). The model wind stress

145   parametrization uses the wind speed at 10m height. Unfortunately, compared with observational data from the Stasiun Klimatologi Mempawah (http://iklim.kalbar.bmkg.go.id), measured at 10 m above the surface, there are clear difference in amplitude. The observed wind velocity is more significant than the wind velocity from ERA5 during a wind surge (Fig. 4). Therefore, in the case study, we adjust the magnitude of the wind input data (ERA5) during the wind surge event. We multiplied the wind magnitude with a ratio between both peaks (the observed and ERA5 data).

150   Next, we set the bulk drag coefficient to 2.5×10^{-3} over the ocean and 1.9×10^{-2} (average bulk drag during December 2018, since it is slightly increasing with the river discharge) over the river part (Kästner et al., 2018). Both coefficients correspond to a sandy bed. Over the dry area, the drag coefficient is determined by two types of land cover (urban and non-urban area), as defined in the Copernicus Global Land Cover map (Buchhorn et al., 2020). For the urban area, the bottom drag coefficient is 2.05 (Hashimoto and Park, 2008). Over the non-urban area, it is set to 2.0, which corresponds to dense vegetation

155   (Li and Busari, 2019).

Then, we imposed discharge at the rivers and tides at the open ocean for the open boundaries. Upstream of the rivers, we imposed the discharge of the Kapuas River and the Landak River. Since there are no observational data for both rivers, we set constant discharges for the simulations in some scenarios. However, to reconstruct the observed inundation (discussed in the case study), we imposed the discharges obtained from the Global Flood Monitoring System (GFMS). GFMS estimated the

160   global discharge based on TRMM Multi-satellite Precipitation Analysis and Global Precipitation Measurement (Wu et al., 2014). The Kapuas River discharge is bigger than the Landak River discharge (Fig. 4). At the open boundaries in the ocean, we prescribed tidal elevation and current of 15 harmonics from the global tides model dataset, the OSU TPXO Tide Models/TPXO9-atlas (Egbert and Erofeeva, 2002). We also retrieved global ocean circulation from HYCOM (Chassignet et al., 2007) at these boundaries.

165   To evaluate the model performance, we performed the tidal analysis on the simulated surface elevation and compared it to the observed water level at the tide gauges. The analysis was conducted using the Unified Tidal Analysis (UTide) Python package (Codiga, 2011). The tidal analysis assumes that a tidal signal is a linear combination of multiple sinusoidal signals associated with its astronomical forcing. Each of these signal components has a different phase, amplitude, and temporal frequency. The analysis aims to obtain tidal harmonic constituents. Since we only ran the model for a limited time duration (in order to

170   minimize the computational cost), it is impossible to extract all tidal constituents from the model's signal output. As a rule of thumb to select the appropriate tidal constituent, we used the Rayleigh criterion (Godin, 1970). Based on this criterion, we

obtained nine tidal constituents with satisfying frequencies, i.e., K1, O1, Q1, P1, J1 (as the representation of the diurnal components) and M2, S2 (as the representation of the semidiurnal components), also MK3 and MO3 (as the representation of the third-diurnal constituents).

175 To perform tidal analysis, water level signals were extracted and analyzed at two points. The first point is located at the river mouth (0.0617N, 109.1751E), and the second point (-0.020431S, 109.338520E) is located along the Kapuas Kecil River within the city of Pontianak (Fig. 1). The second point is located about 20km from the river mouth. At the first point, the model's output signal is compared with the tidal signal from the Indonesian Consortium of Oceanic and Atmospheric Prediction (ina-COAP) (Online Tide Prediction / Prediksi Pasang Surut (Pasut) Online, 2021). Meanwhile, for the second point, the model's

180 signal output is compared to the observational data collected by the Pontianak Maritime Meteorological Station (PMMS).

To quantify the agreement between the simulated water level and observation, we calculated Nash-Sutcliffe Efficiency (NSE) and Root Mean Square Error (RMSE) between both time series along the river within the city. The former coefficient measures how well the model's performance represents the observed data. NSE = 1 represents a perfect model, NSE = 0 depicts a model with a predictive skill the same as the mean of the observed data, and NSE < 0 informs that the mean of the observed data is a

185 better predictor than the model output. The latter coefficient indicates the average of the difference of the peaks between both time series. Both of these coefficients were calculated using the library HydroGof in R (Zambrano-Bigiarini, 2020).

In order to better investigate the inundation extent and depth over the city of Pontianak, we used the HEC-RAS model (HEC-RAS, 2022). We firstly created a new mesh to cover the computational domain over the city and used water levels from the SLIM output model as the boundary conditions (Fig. 12). The new mesh has a 10 m resolution; hence it can better represent

190 canals that spread in the city. Like the SLIM model, the HEC-RAS model also solves the Shallow Water Equations (SWE).

3. Results

3.1 Model validation

The validation results show a good agreement between the model output and the ina-COAP's tidal signal at the Kapuas Kecil river mouth (0.0617N, 109.1751E), with a coefficient of determination $R^2 = 0.95$ and RMSE = 0.09m. At this point, the model

195 produces a tidal signal that has constituents attribute (phase and amplitude) similar to the ina-COAP's tidal signal. The diurnal components explain about 90.69% of the total variances of the estuary's tidal dynamics, while the semidiurnal components only account for about 9.31%, and the shallow water terdiurnal components explain the rest (Fig. 5 and Appendix Table A1 for more detail). Next, the tidal analysis result at the observation point in Pontianak (-0.020431S, 109.338520E) also shows a good agreement between the model output and observation with a coefficient of determination $R^2 = 0.83$ and RMSE = 0.14m.

200 The model output signal also has similar constituents attributed to the PMMS observational water level signal (Fig. 6 and Appendix Table A2). At this point, the diurnal components explain about 89.6% of the total variances of the estuary's tidal dynamics, which is lower from the river mouth. Then, the semidiurnal components account for about 9.9% and the shallow water terdiurnal components explain the rest, which slightly higher than in the river mouth. The analysis at this second point also confirms that the model successfully reproduces the observed hydrodynamics.

205 **3.2 The impact of river discharges on the river's maximum water level.**

The impact of the Kapuas River upstream discharge on its downstream hydrodynamics is assessed by imposing different discharge values ranging from 3,000 m^3/s to 9,000 m^3/s (the highest discharge set based on the simulated data in 2018, see Fig. 4 and Table A3). From these values, only 17% will divert to the Kapuas Kecil branch, while 83% of it continues to flow through the Kapuas Besar (Kästner and Hoitink, 2019). At the same time, the Landak River upstream discharge is set to 300 210 m^3/s for all scenarios, and the tide used in the ocean part is retrieved from TPXO for December 2018 with a tidal range of 1.8 m at the river mouth. The maximum water level (MXWL) at different points along the Kapuas Kecil River stream is then calculated for these different discharge scenarios (Fig. 7). Based on these MXWL profiles, we thus know that the river discharge dominates the maximum water level from the upstream river input to about 46 km before the river mouth. The MXWL profile linearly increases with the discharges. The water level fluctuation in this stream part is therefore river-215 dominated. Then, from this point to a point located at about 4 km from the river mouth, all MXWL profiles start to drop, indicating that there is a compounding effect of the discharge and the tide. The MXWL profile does not increase linearly due to the increase of discharge from the upstream. The different discharge scenarios have a different MXWL distribution pattern in this area. In the lowest discharge scenario, the MXWL profile decreases until about 6 km before the river mouth. Then, it starts to increase gradually and is stable at 4 km before the river mouth. On the other hand, in the highest scenario, the MXWL 220 profile constantly decreased until a point 4 km before the river mouth, then remained steady. In addition, the closer the flow to the river mouth, the lower the gap between the MXWL profiles. This stream part, where both the river discharge and the tide control the MXWL, is called a mixed-energy region. Meanwhile, at about 4 km from the river mouth, the discharge variations have almost no influence the MXWL. In this area, the tides fully control the MXWL. Therefore, this part of the river can be characterized as tidally-dominated.

225 **3.3 The impact of wind surges on the river's maximum water level**

To evaluate the storm surge effect, we consider wind velocity scenarios (Fig. 8). For each scenario, we multiplied the wind velocity over the domain during the inundation event by a constant value ranging from one to five (Table A3). Then, we

evaluated their impact on the MXWL profiles. Based on the profiles (Fig. 9), we thus know that the storm surge strongly dominates the MXWL from the river mouth to about 4 km up the river. The increasing wind velocity directly increases the

230 MXWL distribution profile. The stronger the wind velocity, the higher the MXWL is. Furthermore, from about 4 km to about 7 km of the river mouth, if the wind velocity is set to more than three times its average, the MXWL profile will drop along this area. The stronger the wind velocity, the sharper the decrease is. The decline of the MXWL profile could be due to the fact that the water levels within the river are higher than its riverbanks and then outflows to the floodplain. The outflow to floodplains leads to a reduction in the water levels in the main river.

235 Besides the wind velocity, the flood duration and flood extent along the river are also influenced by the storm duration (Höffken et al., 2020). Figure 10 shows that the impact of the wind surge duration on the maximum water level is not too significant. Still, it makes the flooding event longer—backwater that comes from the river mouth upstream stays longer inland before flowing back to the ocean.

3.4 A case study: analysis of the flood event on 29 December 2018

240 Based on the water level observed by the Pontianak Maritime Meteorological Station (see Fig. 1 for the location), on 29 December 2018, there was a significant increase in water levels from 05.20 UTC to 07.50 UTC. The maximum water level reached 2.8 meters and produced a significant inundation in the city of Pontianak. In order to investigate the main drivers of the event, we simulated the hydrodynamical process along the land-sea continuum for the full month of December 2018. We simulated the hydrodynamical process without and with storm surge scenarios when the expected tidal range during the event

245 is 1.8 m. Since there was no observed discharge upstream during the date, we imposed the river discharge retrieved from GFMS for Kapuas and Landak rivers (Table A3).

The validation result shows that the NSE is 0.82, indicating that the model has a good performance. The RMSE of its peaks is 0.04 m. These results suggest that the model correctly reproduces the actual hydrodynamic processes. The inundation event on 29 December 2018 is well depicted by the model (Fig. 11, light grey box area). The observational data profile (black) shows

250 that the water level dynamic is at the peak moment during the event, where its top seems lower than the previous peak period. The water level dynamic is about to go down when suddenly a strong force pushes it to go up again for a short moment. The storm alone is responsible for a 30 cm increase in the water level during this short moment (light grey box in Fig. 11). After this additional forcing effect disappeared, the water level then decreased steeply and started following the tidal signal again.

A more qualitative validation of the model has also been performed by comparing the extent of the simulated inundation area

255 with observations reported by the local media (Madrosid, 2018). The report mentioned some areas that were confirmed as inundated when the flooding occurred (represented by the red dots in Fig. 13). The report mentioned some areas confirmed as

inundated when the flooding occurred (represented by the red dots in Fig. 13). As a result, our model output validated that these areas were flooded during the flooding event.

We further investigated the inundation extent and depth over the city of Pontianak using the output of the HEC-RAS model. From the model outputs, we thus know that the extent of this inundation reached lowland within the city located far from the riverbanks (Fig. 13). The overtopped water flooded densely populated areas near riverbanks and propagated much further into the city through the drainage channels. In the west part of the city, flood impacts major areas near riverbanks. While in the east part, the major flooded areas fall in lowland areas, located between the Kapuas Kecil and the Landak river streams (The district of Pontianak Timur), and portion the lowland area in the northeast. Next, the peak of the flooding event occurred during a short period. It started at 02.00 UTC and peaked at 07.00 UTC. After 11.00 UTC, most areas were not flooded anymore, while minor areas were ongoingly inundated until 23.00 UTC. At the peak moment, the area inundated was about 1.4×10^4 km2 (Fig. 14), in varying depths.

4. Discussion

Based on the discharge scenarios, we found that the city of Pontianak is located in the mixed-energy region. The maximum water level of the river in the city is therefore controlled by the interaction between discharges from the upstream, storm surge, and tides from the ocean altogether. Consequently, to assess the inundation hazard in the city, the compound flooding scenario approach becomes more appropriate than only single-source flooding scenarios (only coastal, urban, or riverine flooding). Next, we also found that an extreme West Wind velocity with a magnitude greater than 9 m/s can drive the seawater into the river channels based on the wind surge scenarios. As the storm surge continues to push the water upstream, the pile-up water in the estuary will enter the river stream and propagate over several kilometers. If the water propagation is in cooccurrence with high river discharge, the water level can hence overtop riverbanks and lead to a compound inundation over the floodplain. Furthermore, the wind velocity less than 9 m/s or more than 24 m/s (not shown), it does not impact the MXWL profile in the mixed-energy region anymore. These thresholds become minimum and maximum wind velocities that impact the MXWL profile inside the zone. In the thresholds, the change of the MXWL profiles between the wind velocity in 3rd scenario (wind speed = 14.7 m/s) and 4th scenario (wind speed = 19.6 m/s) is somehow more significant than the other MXWL profile changes. Unfortunately, we could not define the zone border between river-dominated and mix-energy regions with this wind scenario. To obtain this border under the wind surge effect, we need to extend the river domain further upstream. We leave this to a future study.

On 29 December 2018, rainfall over the city of Pontianak was less than 7 mm, so that the effect of excessive rainfall could be
285 ruled out in this event. Meanwhile, an intense wind velocity was observed over the coastal area for a few hours. The radar data
shows Cumulonimbus convective clouds formed and moving eastward from the Karimata Strait towards the land (see
Appendix Fig. B1). Cumulonimbus is a cloud type that could produce wind surges, tornadoes, and excessive rainfall (Cotton
et al., 1992). These clouds reached and covered the Kapuas River's mouth on the date, from 04.30 UTC to 05.25 UTC.
Therefore, these clouds most likely triggered a storm over the coastal area with a wind speed ranging from 13 m/s to 21 m/s.
290 The wind direction was oriented from the west to the east during the event. Hence, the total wind effect became the combination
of the direct wind stress effect and the indirect wave run-up effect. Consequently, it drove the water column from the ocean to
the west coast of Borneo island, where the Kapuas estuary is located. Then, the wind piled up the tidal waters inside the Kapuas
river mouth. The piled-up water then propagated from the river mouth to the upstream and was coincidentally met with a high
river discharge. This phenomenon created an increasing water level and caused a short-duration overflow over the floodplain.
295 Therefore, using this scenario, we suggest that the main trigger for the compound inundation, which occurred on 29 December
2018, was an interaction between a storm surge at the estuary area and a high discharge from the Kapuas River.

As with all modeling studies, there are some limitations related to the model that should be mentioned. Firstly, many different
compound flooding schemes possibly occur in this area that has not yet been simulated. Therefore, the delineation of the
compound flooding risk zones based on the MXWL proposed for the Kapuas Kecil River needs further investigation in the
300 future. Secondly, we have not yet imposed excessive rainfall scenarios in the model so that the model only depicts inundation
processes as the effect of the river discharges, tides, and wind surge. In the actual case, a single excessive rainfall is enough to
trigger urban flooding over the floodplain area. Next, the computational domain does not cover the whole dry land over the
delta. It is only limited to Pontianak and the Kapuas Kecil riverbanks from the city to the river mouth. Consequently, the
simulation might not wholly describe the inundation processes and the real extent of the inundated area. These limitations
305 aspect will be improved in future work.

Regarding the event's impact on 29 December 2018, the compound inundation occurred on a day of low precipitation.
Therefore, the residents were not aware and not prepared for such a significant flood event. Even though it happened only for
a short period, the economic loss was severe (Madrosid, 2018). Such loss can hopefully be avoided after the local water
management installs a flood warning system built based on our proposed models.

5. Conclusion

In this study, a model that depicts the Kapuas River's hydrodynamic processes and its interaction with the Karimata Strait tides and wind surges has been successfully set up. We simulated the hydrodynamic processes during extreme events using the model and assessing their impact on the maximum water level along the Kapuas Kecil river. We found that wind surges over the Kapuas Kecil estuary can raise the water level up to 46 km upstream. If the backward water propagation occurs during high river discharges, it can significantly increase the river water level and trigger an inundation over the floodplain, including the city of Pontianak.

Next, we split the main branch of the Kapuas River (Kapuas Kecil River's stream) into three regions based on the maximum water level profiles. From the river mouth to about 4 km up the river is the tidally-dominated region, where the river discharges levels do not impact the maximum water level anymore. From about 4 km to 46 km is the mixed-energy region, where the maximum water level is influenced by the interaction between the tides and the river discharges. Then, from about 46 km upstream is the river-dominated region, where ebbs no longer impact the maximum water level. The local water management can use this zoning category in assessing and mitigating the compound flooding hazard along the riverbanks.

Lastly, as a study case, the factors that drive the inundation event over Pontianak on 29 December 2018 have been successfully investigated. The wind surge, which occurred in the estuary area, was concluded as the main trigger of the flood event. This wind surge pushed seawater upstream and met with a high river discharge, therefore triggering a short inundation event over the floodplains, especially the city of Pontianak.

Acknowledgment

The PhD fellowship of Joko Sampurno is provided by Indonesia Endowment Fund for Education (LPDP) under Grant No. 201712220212183. Computational resources have been provided by the supercomputing facilities of the Université catholique de Louvain (CISM/UCL) and the Consortium des Équipements de Calcul Intensif en Fédération Wallonie Bruxelles (CÉCI) funded by the Fond de la Recherche Scientifique de Belgique (F.R.S.-FNRS) under convention 2.5020.11 and by the Walloon Region.

References

DEMNAS: https://tanahair.indonesia.go.id/demnas/#/, last access: 1 January 2022.

BATimetri NASional: https://tanahair.indonesia.go.id/demnas/#/batnas, last access: 14 July 2021.

Bevacqua, E., Vousdoukas, M. I., Zappa, G., Hodges, K., Shepherd, T. G., Maraun, D., Mentaschi, L., and Feyen, L.: More meteorological events that drive compound coastal flooding are projected under climate change, Commun. Earth Environ. 2020 11, 1, 1–11, https://doi.org/10.1038/s43247-020-00044-z, 2020.

Bilskie, M. V. and Hagen, S. C.: Defining Flood Zone Transitions in Low-Gradient Coastal Regions, Geophys. Res. Lett., 45, 2761–2770, https://doi.org/10.1002/2018GL077524, 2018.

Buchhorn, M., Lesiv, M., Tsendbazar, N.-E., Herold, M., Bertels, L., and Smets, B.: Copernicus Global Land Cover Layers— Collection 2, Remote Sens. 2020, Vol. 12, Page 1044, 12, 1044, https://doi.org/10.3390/RS12061044, 2020.

Chassignet, E. P., Hurlburt, H. E., Smedstad, O. M., Halliwell, G. R., Hogan, P. J., Wallcraft, A. J., Baraille, R., and Bleck, R.: The HYCOM (HYbrid Coordinate Ocean Model) data assimilative system, J. Mar. Syst., 65, 60–83, https://doi.org/10.1016/J.JMARSYS.2005.09.016, 2007.

Codiga, D. L.: Unified Tidal Analysis and Prediction, Graduate School of Oceanography, University of Rhode Island, Narragansett, RI., 59 pp., 2011.

Cotton, W. R., Bryan, G., and Heever, S. C. van den: Cumulonimbus Clouds and Severe Convective Storms, in: International Geophysics, vol. 44, Academic Press, 455–592, https://doi.org/10.1016/S0074-6142(08)60548-3, 1992.

Deb, M. and Ferreira, C. M.: Potential impacts of the Sunderban mangrove degradation on future coastal flooding in Bangladesh, J. Hydro-Environment Res., 17, 30–46, https://doi.org/10.1016/j.jher.2016.11.005, 2017.

Egbert, G. D. and Erofeeva, S. Y.: Efficient inverse modeling of barotropic ocean tides, J. Atmos. Ocean. Technol., 19, 183–204, 2002.

Think Hazard - Indonesia: https://thinkhazard.org/en/report/116-indonesia, last access: 8 January 2022.

Giloy, N., Hamdi, Y., Bardet, L., Garnier, E., and Duluc, C. M.: Quantifying historic skew surges: an example for the Dunkirk Area, France, Nat. Hazards, 98, 869–893, https://doi.org/10.1007/s11069-018-3527-1, 2019.

Godin, G.: The resolution of tidal constituents, Int. Hydrogr. Rev., XLVII, 1970.

Goltenboth, F., Timotius, K. H., Milan, P. P., and Margraf, J.: Ecology of insular Southeast Asia: the Indonesian archipelago, Elsevier B.V., 2006.

Gourgue, O., Baeyens, W., Chen, M. S., de Brauwere, A., de Brye, B., Deleersnijder, E., Elskens, M., and Legat, V.: A depth-averaged two-dimensional sediment transport model for environmental studies in the Scheldt Estuary and tidal river network, J. Mar. Syst., 128, 27–39, https://doi.org/10.1016/j.jmarsys.2013.03.014, 2013.

Hashimoto, H. and Park, K.: Two-dimensional urban flood simulation: Fukuoka flood disaster in 1999, WIT Trans. Ecol. Environ., 118, 59–67, https://doi.org/10.2495/FRIAR080061, 2008.

Herdman, L., Erikson, L., and Barnard, P.: Storm surge propagation and flooding in small tidal rivers during events of mixed

coastal and fluvial influence, J. Mar. Sci. Eng., 6, 158, https://doi.org/10.3390/JMSE6040158, 2018.

Hersbach, H., Bell, B., Berrisford, P., Hirahara, S., Horányi, A., Muñoz-Sabater, J., Nicolas, J., Peubey, C., Radu, R., Schepers, D., Simmons, A., Soci, C., Abdalla, S., Abellan, X., Balsamo, G., Bechtold, P., Biavati, G., Bidlot, J., Bonavita, M., Chiara, G., Dahlgren, P., Dee, D., Diamantakis, M., Dragani, R., Flemming, J., Forbes, R., Fuentes, M., Geer, A., Haimberger, L., Healy, S., Hogan, R. J., Hólm, E., Janisková, M., Keeley, S., Laloyaux, P., Lopez, P., Lupu, C., Radnoti, G., Rosnay, P., Rozum, I., Vamborg, F., Villaume, S., and Thépaut, J.: The ERA5 global reanalysis, Q. J. R. Meteorol. Soc., 146, 1999–2049, https://doi.org/10.1002/qj.3803, 2020.

Hidayat, H., Hoekman, D., Vissers, M., Hossain, M. M., Teuling, A., and Haryani, G.: Inundation Frequency Mapping of The Upper Kapuas Wetlands Using Radar Imagery, in: INTERNATIONAL CONFERENCE ON ECOHYDROLOGY (ICE), 250–257, 2014.

Höffken, J., Vafeidis, A. T., MacPherson, L. R., and Dangendorf, S.: Effects of the Temporal Variability of Storm Surges on Coastal Flooding, Front. Mar. Sci., 7, 98, https://doi.org/10.3389/FMARS.2020.00098/BIBTEX, 2020.

Hunter, J. D.: Matplotlib: A 2D graphics environment, Comput. Sci. Eng., 9, 90–95, https://doi.org/10.1109/MCSE.2007.55, 2007.

Huybrechts, N. ;, Villaret, C. ;, and Hervouet, J.-M.: Comparison between 2D and 3D modelling of sediment transport: application to the dune evolution, in: River Flow 2010, 887–894, 2010.

Kästner, K. and Hoitink, A. J. F.: Flow and Suspended Sediment Division at Two Highly Asymmetric Bifurcations in a River Delta: Implications for Channel Stability, J. Geophys. Res. Earth Surf., 124, 2358–2380, https://doi.org/10.1029/2018JF004994, 2019.

Kästner, K., Hoitink, A. J. F., Vermeulen, B., Geertsema, T. J., and Ningsih, N. S.: Distributary channels in the fluvial to tidal transition zone, J. Geophys. Res. Earth Surf., 122, 696–710, https://doi.org/10.1002/2016JF004075, 2017.

Kästner, K., Hoitink, A. J. F., Torfs, P. J. J. F., Vermeulen, B., Ningsih, N. S., and Pramulya, M.: Prerequisites for Accurate Monitoring of River Discharge Based on Fixed-Location Velocity Measurements, Water Resour. Res., 54, 1058–1076, https://doi.org/10.1002/2017WR020990, 2018.

Kästner, K., Hoitink, A. J. F., Torfs, P. J. J. F., Deleersnijder, E., and Ningsih, N. S.: Propagation of tides along a river with a sloping bed, J. Fluid Mech., 872, 39–73, https://doi.org/10.1017/JFM.2019.331, 2019.

Lambrechts, J., Humphrey, C., McKinna, L., Gourge, O., Fabricius, K. E., Mehta, A. J., Lewis, S., and Wolanski, E.: Importance of wave-induced bed liquefaction in the fine sediment budget of Cleveland Bay, Great Barrier Reef, Estuar. Coast. Shelf Sci., 89, 154–162, https://doi.org/10.1016/j.ecss.2010.06.009, 2010.

Le, H.-A., Lambrechts, J., Ortleb, S., Gratiot, N., Deleersnijder, E., and Soares-Frazão, S.: An implicit wetting-drying

algorithm for the discontinuous Galerkin method: application to the Tonle Sap, Mekong River Basin, Environ. Fluid Mech., 20, 923–951, https://doi.org/10.1007/s10652-019-09732-7, 2020.

Li, C. and Busari, A. O.: Hybrid modeling of flows over submerged prismatic vegetation with different areal densities, Eng. Appl. Comput. Fluid Mech., 13, 493–505, https://doi.org/10.1080/19942060.2019.1610501, 2019.

400   MacKinnon, K., Hatta, G., Mangalik, A., and Halim, H.: The ecology of Kalimantan. Vol. 3, Oxford University Press., 1996.

Madrosid: Cerita Warga, Detik-detik Banjir Rob Melanda Kota Pontianak, Trib. Pontianak, 2018.

Moftakhari, H. R., AghaKouchak, A., Sanders, B. F., Feldman, D. L., Sweet, W., Matthew, R. A., and Luke, A.: Increased nuisance flooding along the coasts of the United States due to sea level rise: Past and future, Geophys. Res. Lett., 42, 9846–9852, https://doi.org/10.1002/2015GL066072, 2015.

405   Néelz, S.: Desktop review of 2D hydraulic modelling packages, Bristol: Environment Agency, 2009.

Olbert, A. I., Comer, J., Nash, S., and Hartnett, M.: High-resolution multi-scale modelling of coastal flooding due to tides, storm surges and rivers inflows. A Cork City example, Coast. Eng., 121, 278–296, https://doi.org/10.1016/j.coastaleng.2016.12.006, 2017.

Planet dump retrieved from https://planet.osm.org: https://www.openstreetmap.org, last access: 20 October 2020.

410   Patel, D. P., Ramirez, J. A., Srivastava, P. K., Bray, M., and Han, D.: Assessment of flood inundation mapping of Surat city by coupled 1D/2D hydrodynamic modeling: a case application of the new HEC-RAS 5, Nat. Hazards, 89, 93–130, https://doi.org/10.1007/s11069-017-2956-6, 2017.

Kondisi Geografis Kota Pontianak: https://www.pontianakkota.go.id/tentang/geografis, last access: 5 April 2021.

Pham Van, C., de Brye, B., Deleersnijder, E., F Hoitink, A. J., Sassi, M., Spinewine, B., Hidayat, H., and Soares-Frazão, S.:
415   Simulations of the flow in the Mahakam river-lake-delta system, Indonesia, Environ. Fluid Mech., 16, 603–633, https://doi.org/10.1007/s10652-016-9445-4, 2016.

Online Tide Prediction / Prediksi Pasang Surut (Pasut) Online: http://tides.big.go.id/pasut/index.html, last access: 5 April 2021.

Remacle, J. F. and Lambrechts, J.: Fast and robust mesh generation on the sphere—Application to coastal domains, CAD Comput. Aided Des., 103, 14–23, https://doi.org/10.1016/j.cad.2018.03.002, 2018.

420   Santiago-Collazo, F. L., Bilskie, M. V., and Hagen, S. C.: A comprehensive review of compound inundation models in low-gradient coastal watersheds, Environ. Model. Softw., 119, 166–181, https://doi.org/10.1016/J.ENVSOFT.2019.06.002, 2019.

Spicer, P., Huguenard, K., Ross, L., and Rickard, L. N.: High-Frequency Tide-Surge-River Interaction in Estuaries: Causes and Implications for Coastal Flooding, J. Geophys. Res. Ocean., 124, 9517–9530, https://doi.org/10.1029/2019JC015466, 2019.

425   Twilley, R. R., Bentley, S. J., Chen, Q., Edmonds, D. A., Hagen, S. C., Lam, N. S. N., Willson, C. S., Xu, K., Braud, D. W.,

Hampton Peele, R., and McCall, A.: Co-evolution of wetland landscapes, flooding, and human settlement in the Mississippi River Delta Plain, Sustain. Sci., 11, 711–731, https://doi.org/10.1007/s11625-016-0374-4, 2016.

HEC-RAS: https://www.hec.usace.army.mil/software/hec-ras/, last access: 8 January 2022.

Vallaeys, V., Kärnä, T., Delandmeter, P., Lambrechts, J., Baptista, A. M., Deleersnijder, E., and Hanert, E.: Discontinuous
430   Galerkin modeling of the Columbia River's coupled estuary-plume dynamics, Ocean Model., 124, 111–124, https://doi.org/10.1016/j.ocemod.2018.02.004, 2018.

Vitousek, S., Barnard, P. L., Fletcher, C. H., Frazer, N., Erikson, L., and Storlazzi, C. D.: Doubling of coastal flooding frequency within decades due to sea-level rise, Sci. Rep., 7, 1–9, https://doi.org/10.1038/s41598-017-01362-7, 2017.

Vu, T. T. and Ranzi, R.: Flood risk assessment and coping capacity of floods in central Vietnam, J. Hydro-Environment Res.,
435   14, 44–60, https://doi.org/10.1016/j.jher.2016.06.001, 2017.

Wahyu, A., Kuntoro, A., and Yamashita, T.: Annual and Seasonal Discharge Responses to Forest/Land Cover Changes and Climate Variations in Kapuas River Basin, Indonesia, J. Int. Dev. Coop., 16, 81–100, https://doi.org/10.15027/29807, 2010.

Wells, J. A., Wilson, K. A., Abram, N. K., Nunn, M., Gaveau, D. L. A., Runting, R. K., Tarniati, N., Mengersen, K. L., and Meijaard, E.: Rising floodwaters: Mapping impacts and perceptions of flooding in Indonesian Borneo,
440   https://doi.org/10.1088/1748-9326/11/6/064016, 20 June 2016.

Coastal Flooding Forecast Strengthened in Indonesia | World Meteorological Organization: https://public.wmo.int/en/media/news/coastal-flooding-forecast-strengthened-indonesia, last access: 3 April 2021.

Wu, H., Adler, R. F., Tian, Y., Huffman, G. J., Li, H., and Wang, J.: Real-time global flood estimation using satellite-based precipitation and a coupled land surface and routing model, Water Resour. Res., 50, 2693–2717,
445   https://doi.org/10.1002/2013WR014710, 2014.

Zambrano-Bigiarini, M.: Goodness-of-Fit Functions for Comparison of Simulated and Observed Hydrological Time Series [R package hydroGOF version 0.4-0], 2020.

Zhang, J. and Liu, H.: Modeling of waves overtopping and flooding in the coastal reach by a non-hydrostatic model, in: Procedia IUTAM, 126–130, https://doi.org/10.1016/j.piutam.2017.09.019, 2017.

450   Zijl, F., Verlaan, M., and Gerritsen, H.: Improved water-level forecasting for the Northwest European Shelf and North Sea through direct modelling of tide, surge and non-linear interaction, Ocean Dyn., 63, 823–847, https://doi.org/10.1007/s10236-013-0624-2, 2013.
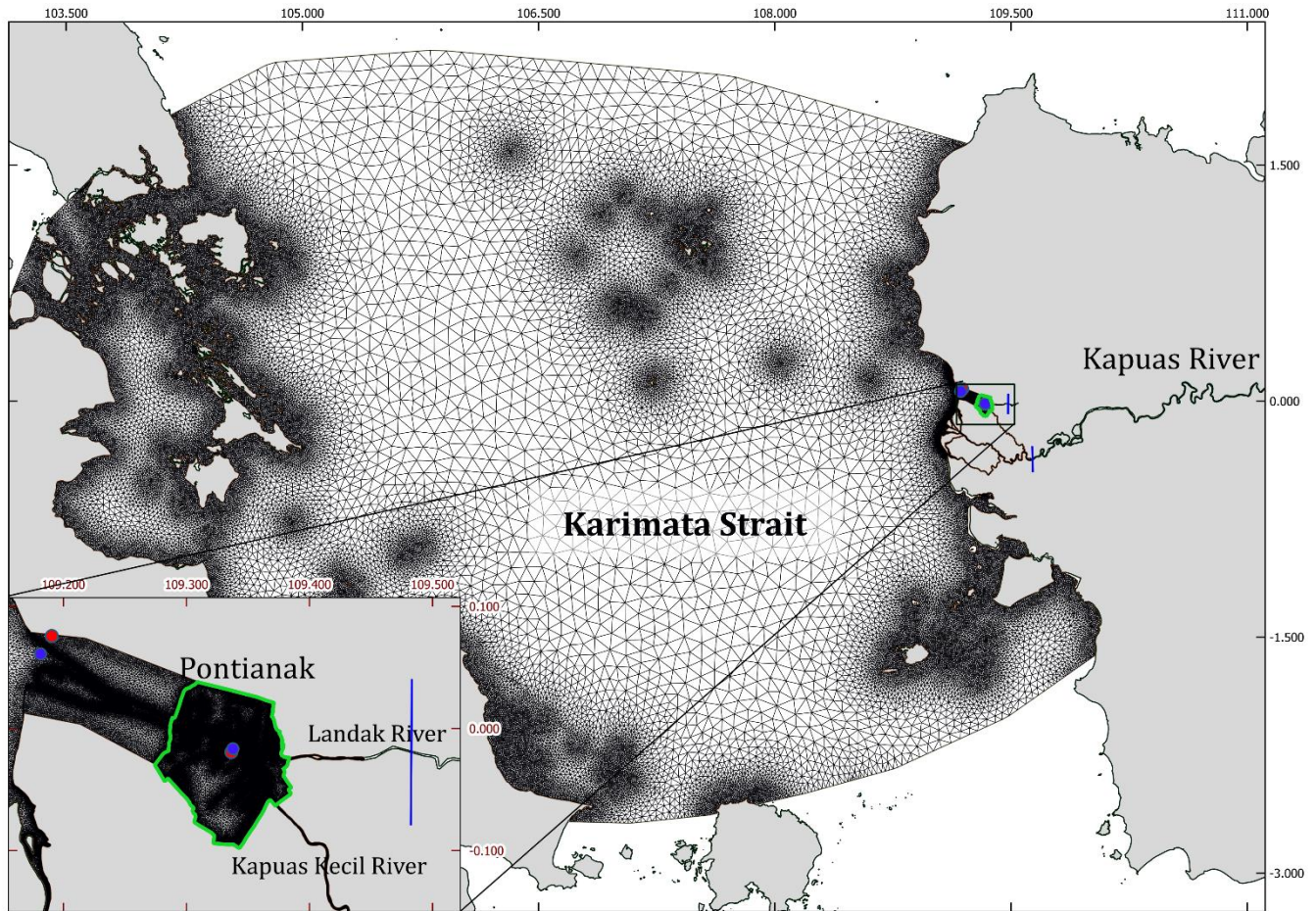
455

Figure 1. The region of interest includes the Karimata Strait, the Kapuas River and its estuary, and the city of Pontianak, whose limits are shown in green. The triangles represent the unstructured mesh of the computational domain, which has a resolution of 50 m over the river and estuary, 1 km near the coastlines, and 10 km in the middle of the Karimata Strait. The mesh is composed of 206,359 triangular elements. Red dots represent the weather station's locations, and blue dots represent the tidal validation points (left: river mouth, right: Pontianak

460 Maritime Meteorological Station observation point). Blue lines depict the river boundary where discharges are imposed in the model. Background map retrieved from (Planet dump retrieved from https://planet.osm.org, 2020). © OpenStreetMap contributors 2017. Distributed under the Open Data Commons Open Database License (ODbL) v1.0.

465
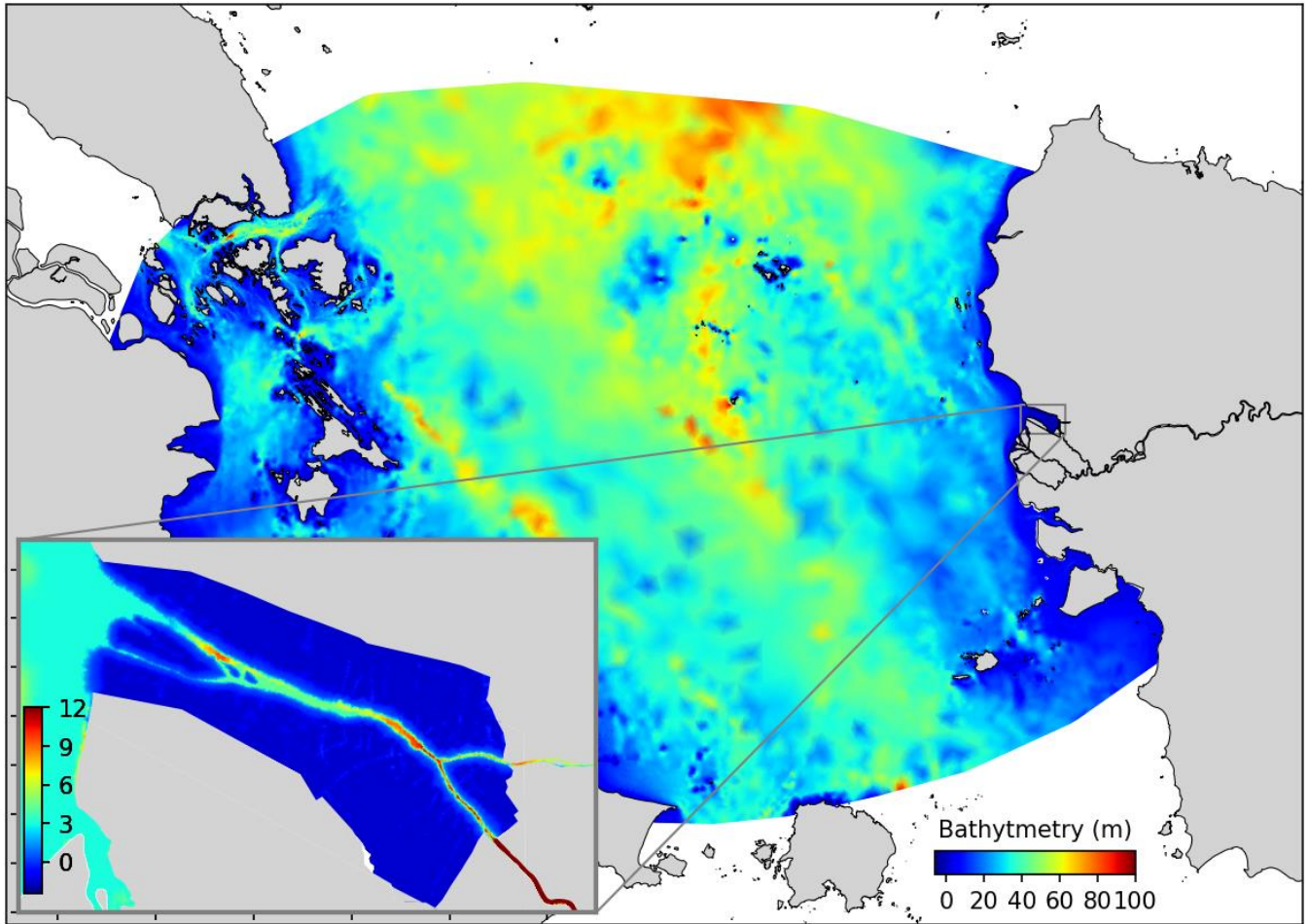
Figure 2. Bathymetry map, where positive values mean under the mean sea level. Background map created using python library: matplotlib (Hunter, 2007).

470

475
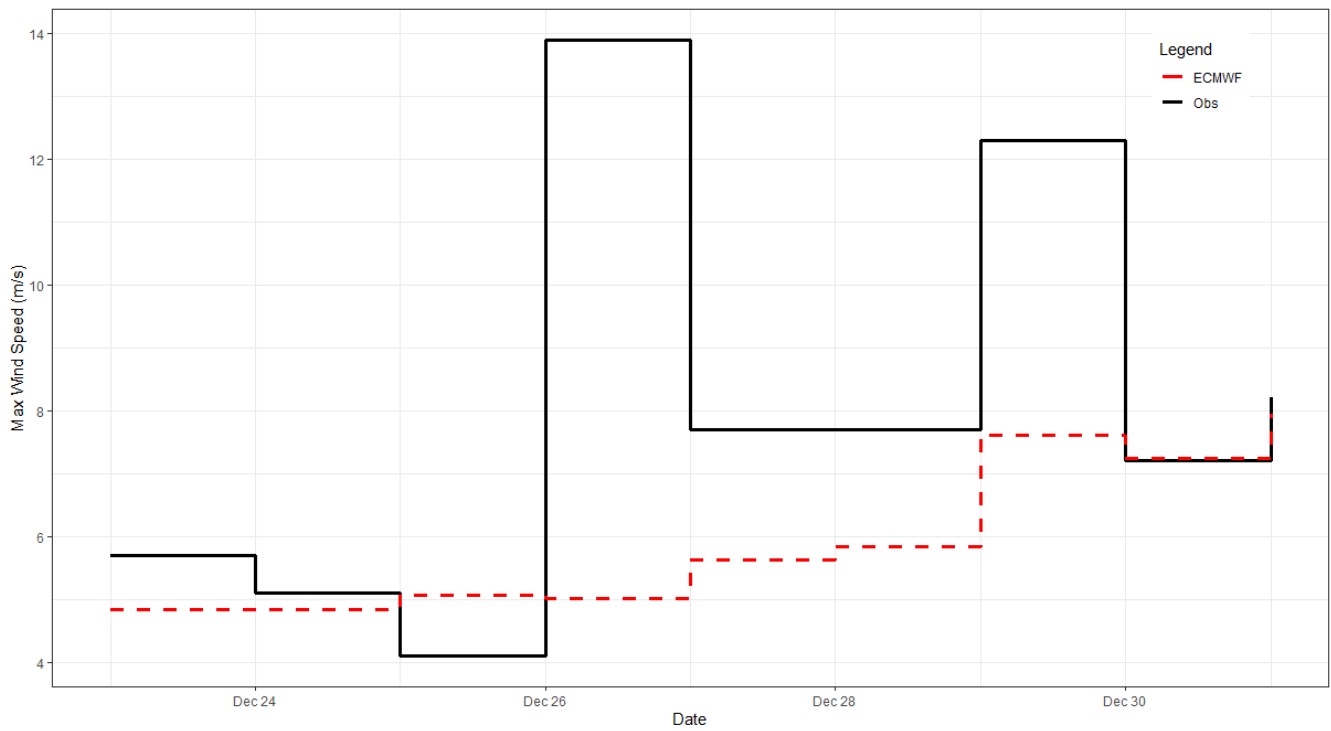
480

Figure 3. The daily maximum wind ERA5 dataset compared to the observation data at the Kapuas Kecil river mouth. It is shown that during the wind surges, the ERA5 wind product still underestimates the observation data.
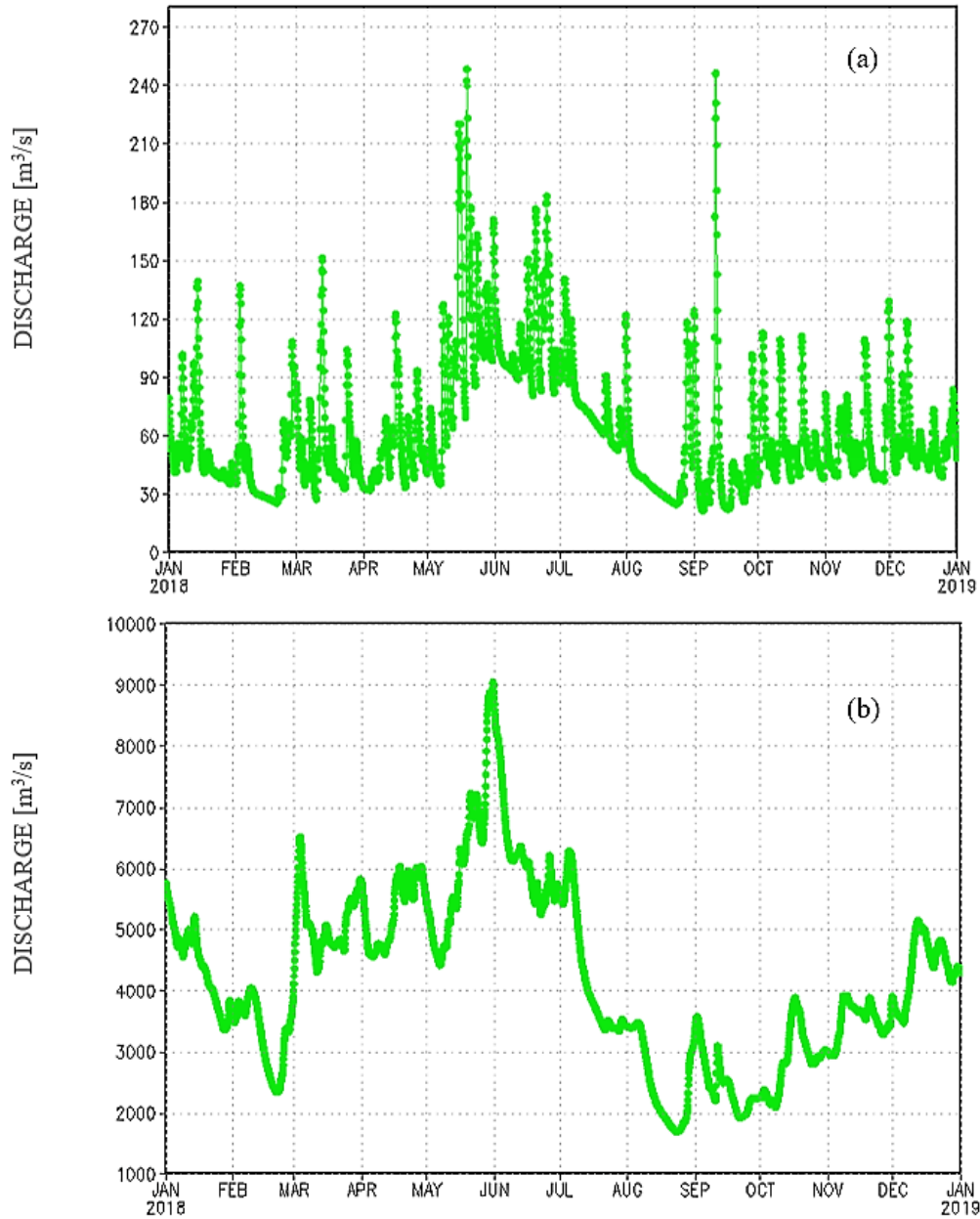
Figure 4. River discharge of (a) the Landak (prescribed at coordinate 0.0282S, 109.445E) and (b) the Kapuas (prescribed at coordinate 0.3623S, 109.6394E) retrieved from (Wu et al., 2014).
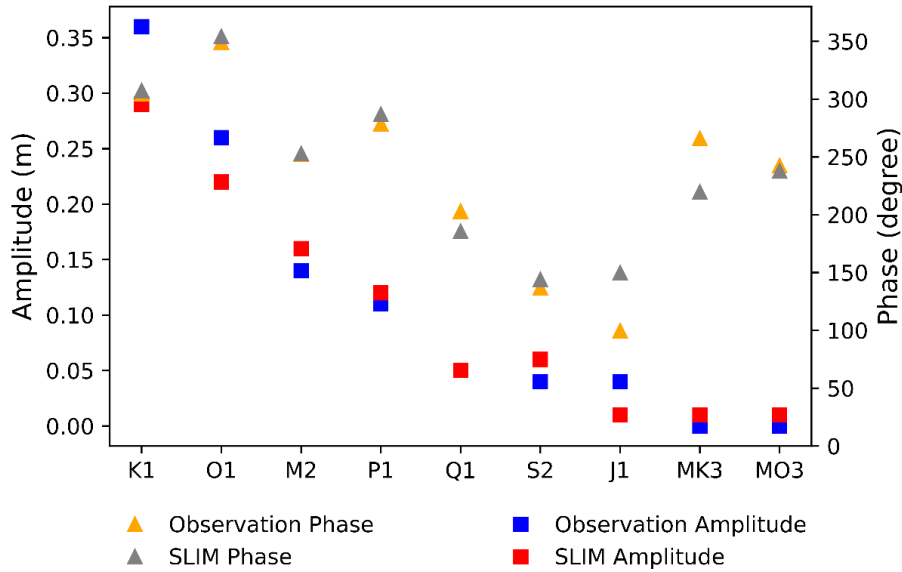
Figure 5. Observed and simulated tidal constituents (amplitude and phase) at the Kapuas Kecil river mouth (0.0617N, 109.1751E) during December 2018.

490
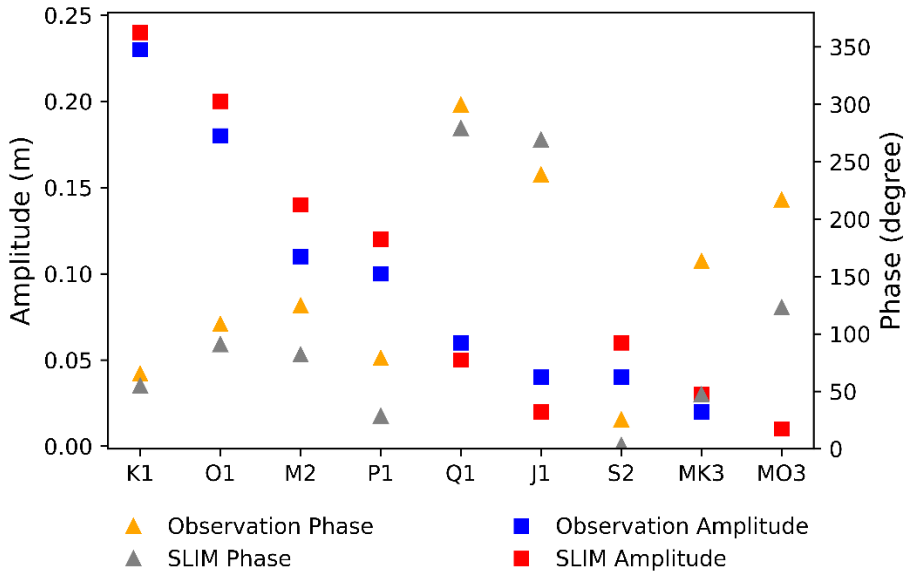
Figure 6. Observed and simulated tidal constituents (amplitude and phase) at the Middle of Pontianak (-0.020431S, 109.338520E) during December 2018.
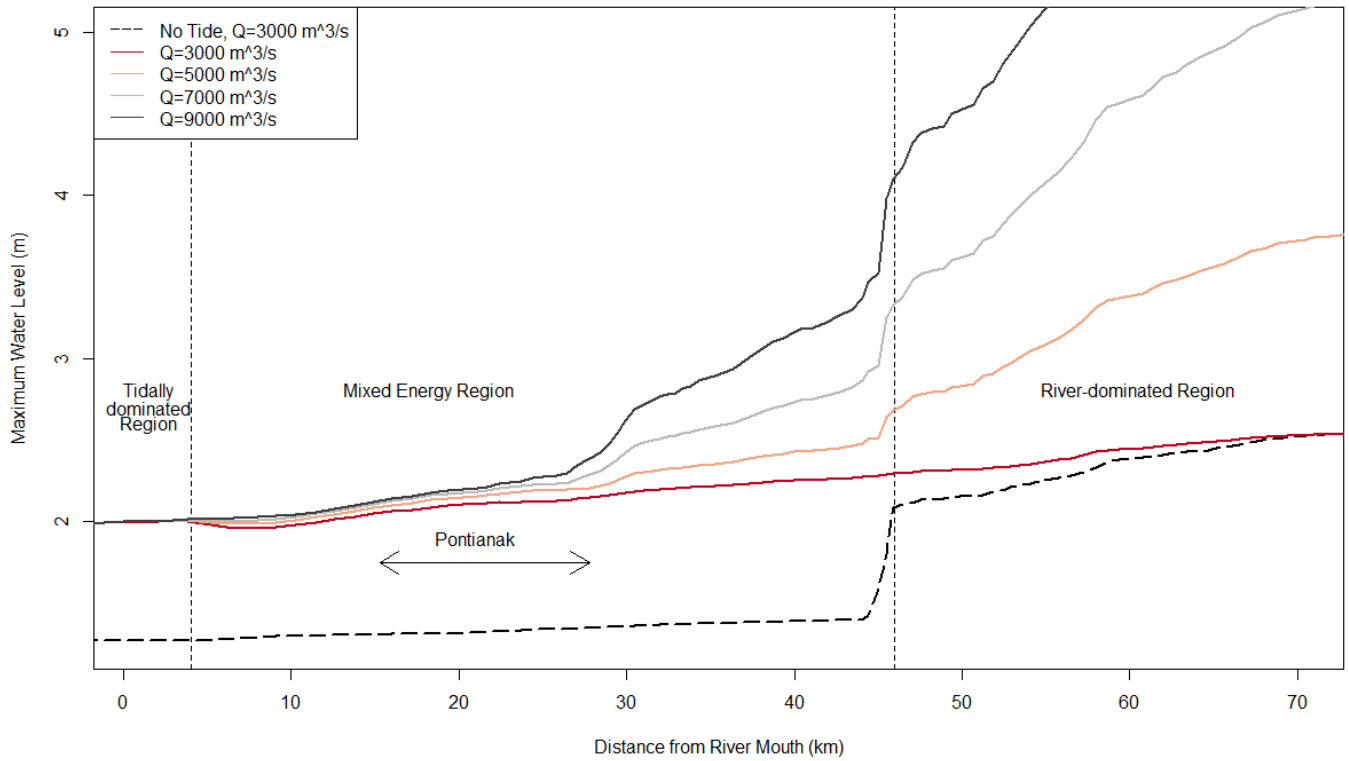
Figure 7. River discharge affects the maximum water level (MXWL) with respect lowest astronomical tide (LAT). Black dash vertical lines are the border between the tidal-fluvial region. The arrow shows the river stream that flows inside Pontianak, where the population is the densest in the domain.
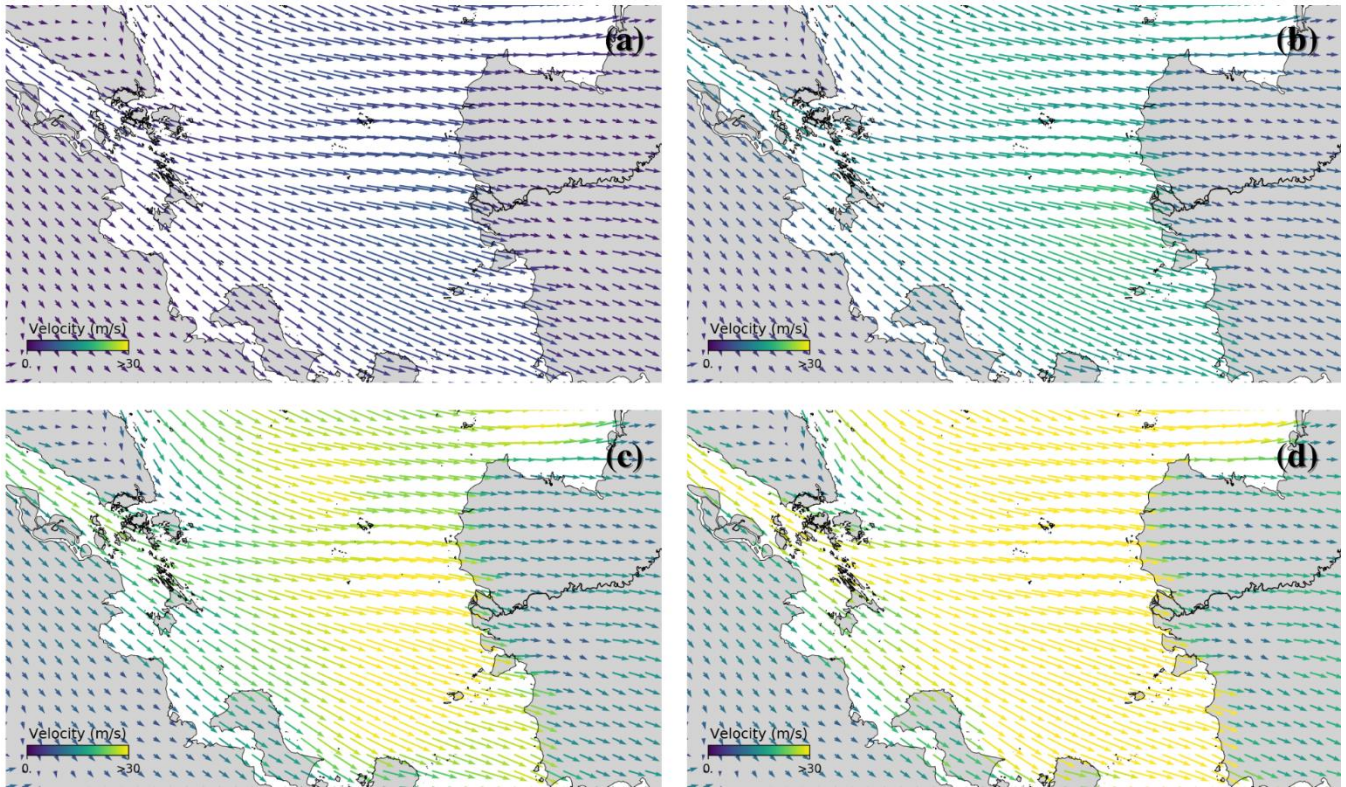
Figure 8. Wind direction and magnitude over the domain for (a) scenario Wind1x, (b) scenario wind 2.5x, (c) scenario wind 4x, and (d) scenario wind 5x. Background map created using python library: matplotlib (Hunter, 2007).

500
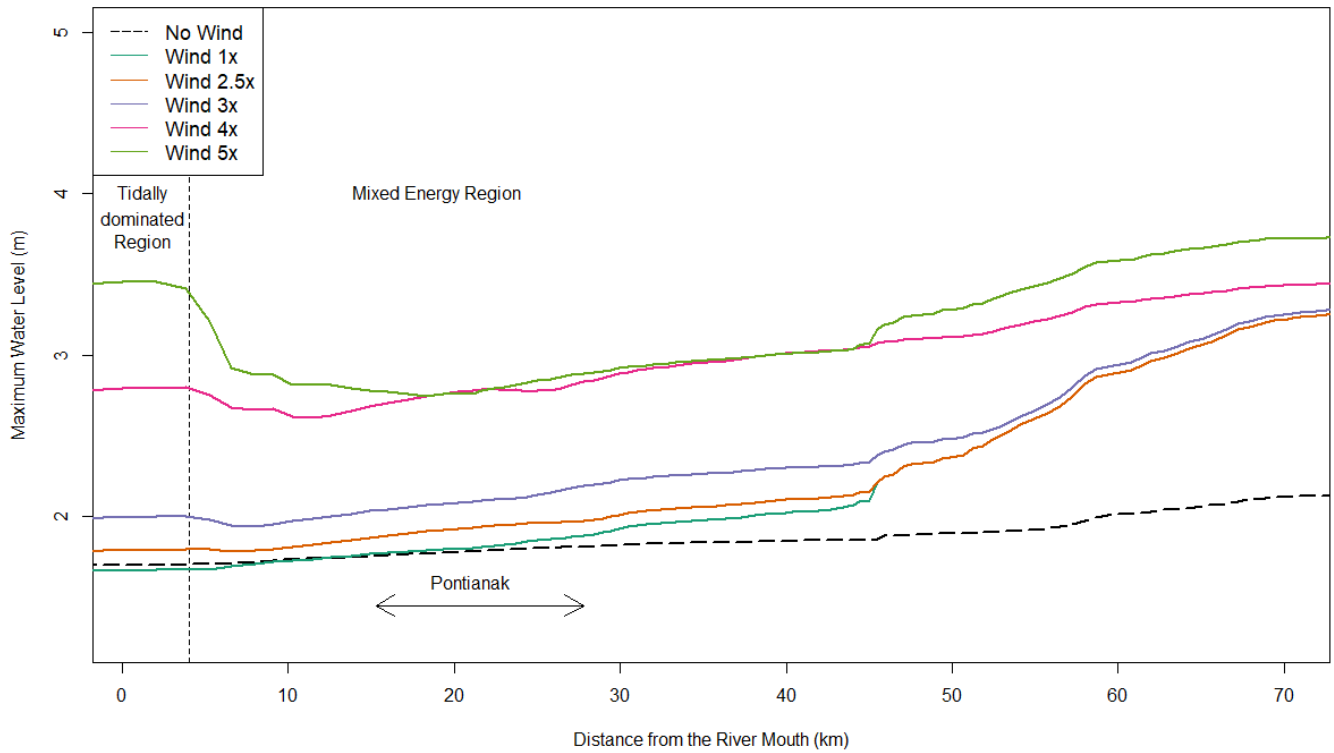
Figure 9. Wind surge affects the maximum water level (MXWL) with respect lowest astronomical tide (LAT), where the black dash vertical line is the border between the tidal-fluvial regions. The arrow shows the river stream that flows inside Pontianak.
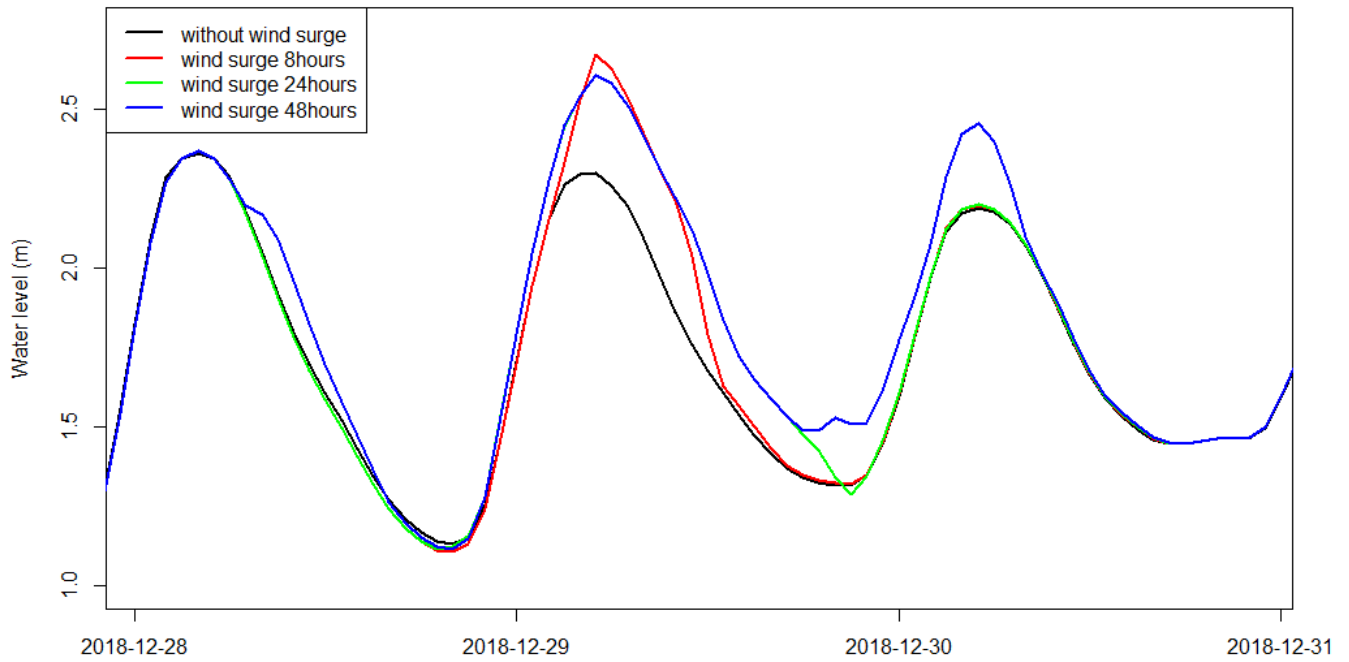
Figure 10. Wind surge duration affects the increasing of water level in Pontianak.
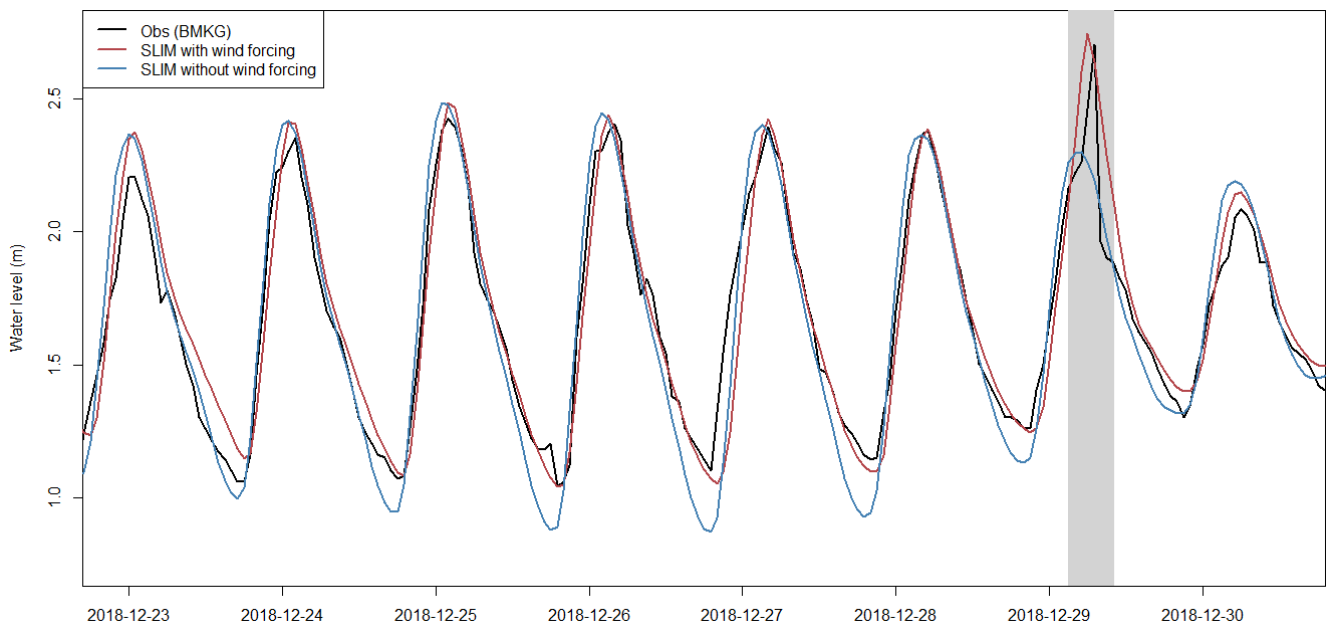
Figure 11. Validation of water level at Pontianak, where light grey box depicts the peak of the inundation

505
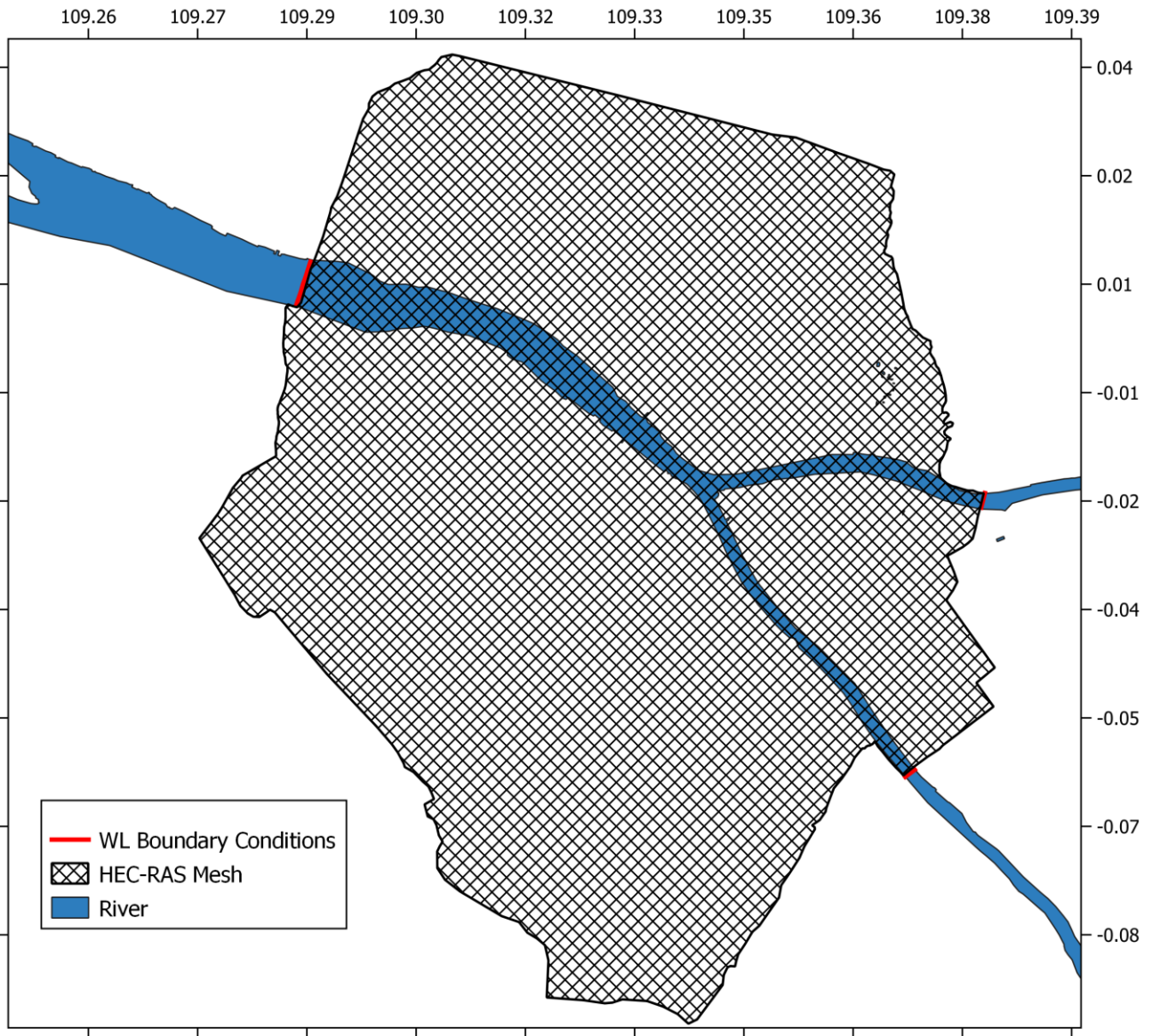
Figure 12. HEC-RAS 2D mesh with a resolution of 10 m for flood extent analysis in the city of Pontianak.
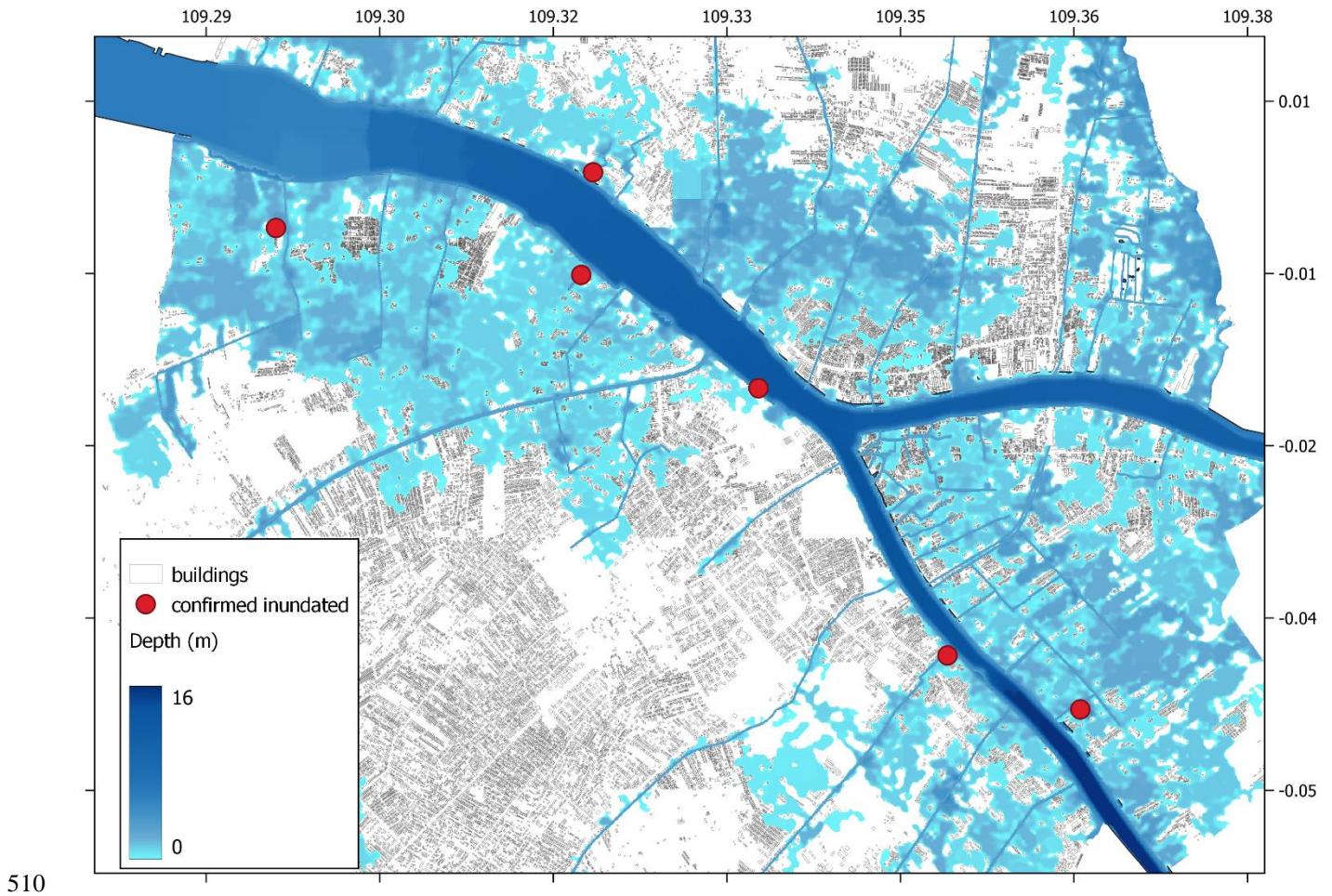
Figure 13. Inundation extent map and its depth during the flood event on the 29 December 2018 at 06.00 UTC. The red dots represent places that were reported as inundated during the event. City's building map retrieved from (Planet dump retrieved from https://planet.osm.org, 2020). © OpenStreetMap contributors 2017. Distributed under the Open Data Commons Open Database License (ODbL) v1.0.
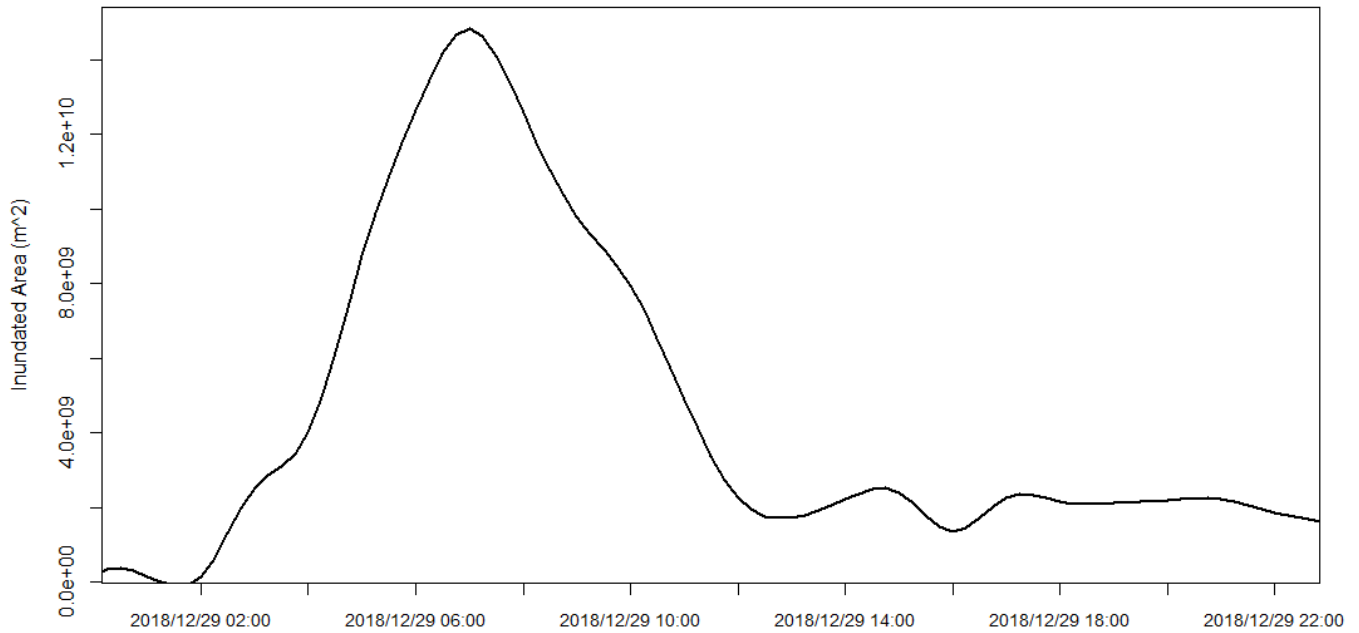
Figure 14. The total inundated area within the city of Pontianak during the flood event on 29 December 2018

520 **Appendix**

A. Detail on the tidal constituents

The amplitude, phase and energy of each tidal constituent at the river mouth and in Pontianak are summarized in Table A1 and A2.

Table A1. Tide Constituents at the Kapuas Kecil River mouth (0.0617N, 109.1751E) in December 2018**.**

Tidal constituent	inaCOAP			SLIM			Error		Rayleigh Criterion
	Amplitude (m)	Phase (^{0})	Percent Energy (%)	Amplitude (m)	Phase (^{0})	Percent Energy (%)	ΔAmplitude (m)	ΔPhase (^{0})	
K1	0.36	304.59	54.39	0.29	307.29	48.03	0.06	2.71	0.16
O1	0.26	349.21	29.56	0.22	353.95	27.30	0.04	4.75	1.09
M2	0.14	252.24	8.62	0.16	252.74	13.46	0.02	0.50	26.80
P1	0.11	278.45	4.95	0.12	286.67	7.88	0.01	8.22	2.03
Q1	0.05	202.88	1.03	0.05	185.47	1.31	0.00	17.40	24.77
J1	0.04	99.54	0.69	0.01	149.53	0.11	0.03	50.00	1.09
S2	0.04	136.68	0.76	0.06	143.77	1.75	0.01	7.10	2.03
MK3	0.00	265.87	0.00	0.01	219.53	0.06	0.01	46.34	2.20
MO3	0.00	242.35	0.00	0.01	237.60	0.09	0.01	4.75	25.85

Table A2. Tide Constituents at the middle of Pontianak (-0.020431S, 109.338520E) in December 2018.

Tidal constituent	Observation			SLIM			Error		Rayleigh Criterion
	Amplitude (m)	Phase (^{0})	Percent Energy (%)	Amplitude (m)	Phase (^{0})	Percent Energy (%)	ΔAmplitude (m)	ΔPhase (^{0})	
K1	0.23	65.24	42.42	0.24	54.85	42.11	0.01	4.65	0.16
O1	0.18	108.39	25.33	0.20	90.81	28.71	0.02	3.64	1.09
M2	0.11	124.73	13.34	0.14	81.92	14.53	0.04	13.83	26.80
P1	0.1	78.8	10.54	0.12	28.50	9.73	0.02	35.35	2.03
Q1	0.06	299.63	4.11	0.05	279.19	1.71	0.01	7.04	24.77
J1	0.04	238.67	1.78	0.02	269.16	0.37	0.02	46.08	1.09
S2	0.04	25.4	1.54	0.06	3.22	2.21	0.02	352.17	2.03
MK3	0.02	163.32	0.52	0.03	47.35	0.46	0.01	71.94	2.20
MO3	0.01	216.89	0.42	0.01	122.99	0.17	0.00	50.98	25.85

Table A3. Scenarios used to force the model.

Scenario	Duration of simulation	Wind Speed (ms^{-1})	Wind Direction (^{o})	Pressure (kPa)	Discharge Kapuas (m^{3}s^{-1})	Discharge Landak (m^{3}s^{-1})	Tidal Range (m)
Discharge1	1 month	2 - 8	0 – 360	100.5 - 101.5	3×10^3	300	1.8
Discharge2	1 month	2 - 8	0 – 360	100.5 - 101.5	5×10^3	300	1.8
Discharge3	1 month	2 - 8	0 – 360	100.5 - 101.5	7×10^3	300	1.8
Discharge4	1 month	2 – 8	0 – 360	100.5 - 101.5	9×10^3	300	1.8
Wind_1x	1 month	2 – 8	0 – 360	100.5 - 101.5	3×10^3	300	1.8
Wind_1.5x	1 month	3 – 12	0 – 360	100.5 - 101.5	3×10^3	300	1.8
Wind_2x	1 month	4 – 16	0 – 360	100.5 - 101.5	3×10^3	300	1.8
Wind_2.5x	1 month	5 – 20	0 – 360	100.5 - 101.5	3×10^3	300	1.8
Wind_3x	1 month	6 - 24	0 – 360	100.5 - 101.5	3×10^3	300	1.8
Wind_4x	1 month	8 - 32	0 – 360	100.5 - 101.5	3×10^3	300	1.8
Wind_5x	1 month	10 - 40	0 – 360	100.5 - 101.5	3×10^3	300	1.8
Case Study	1 month	2 – 21	0 – 360	100.5 - 101.5	$3.3 \times 10^3 - 5 \times 10^3$	250-700	1.8

B. Local weather condition on 29 December 2018
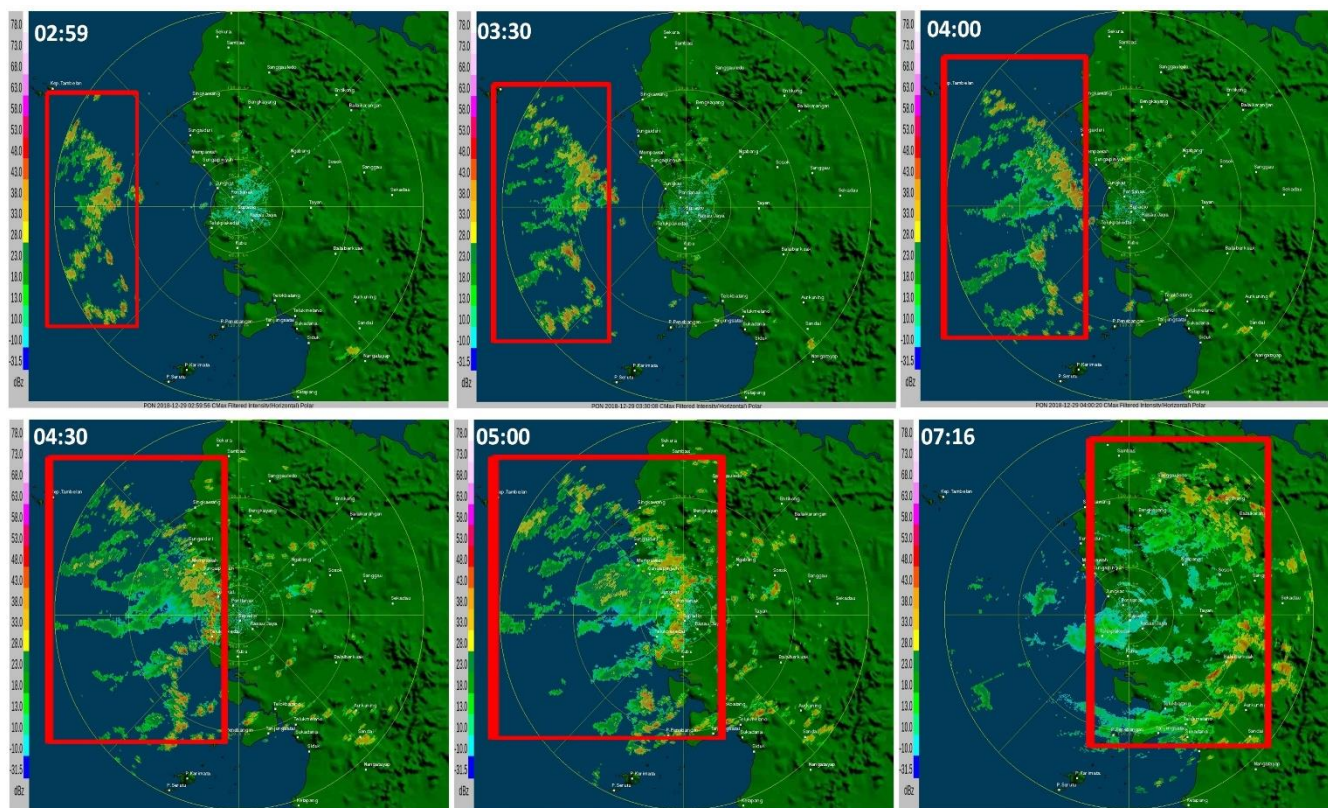
530

Figure B1. Radar data, observed by the Supadio Meteorological Station (http://kalbar.bmkg.go.id/profil/), depicts the clouds' growth and movement (in the red box) on 29 December 2018. The clouds started to grow over the ocean and are pushed by the wind to move eastward at 02.59 UTC. The clouds reach their maximum intensity at 05.00 UTC while located above the Kapuas Estuary. Furthermore, the clouds spread over a wider area with a weakening intensity at 07.00 UTC.

535